The current issue and full text archive of this journal is available on Emerald Insight at:
https://www.emerald.com/insight/2049-6427.htm

Aerodynamic and structural performances of a single-stage transonic axial compressor with blade fillet radius

Hoang-Quan Chu
Faculty of Aerospace Engineering, Le Quy Don Technical University, Hanoi, Vietnam, and
Cong-Truong Dinh
School of Mechanical Engineering, Hanoi University of Science and Technology, Hanoi, Vietnam

Received 23 July 2021
Revised 23 December 2021
Accepted 8 January 2022

Abstract

Purpose – This study's investigation aims to clarify the effect of an additional geometry, i.e. a fillet radius, to the blades of a single-stage transonic axial compressor, NASA Stage 37, on its aerodynamic and structural performances.

Design/methodology/approach – Applying the commercial simulation software and the one-way fluid–structure interaction (FSI) approach, this study first evaluated the simulation results with the experimental data for the aerodynamic performances. Second, this paper compared the structural performances between the models with and without fillets.

Findings – This research analyses the aerodynamic results (i.e. total pressure ratio, adiabatic efficiency, stall margin) and the structural outcomes (i.e. equivalent von Mises stress, total deformation) of the single-stage transonic axial compressor NASA Stage 37.

Originality/value – This paper mentions the influence of blade fillets (i.e. both rotor hub fillet and stator shroud fillet) on the compressor performances (i.e. the aerodynamic and structural performances).

Keywords Single-stage transonic axial compressor, Fillet radius, 3-D RANS, 1-Way FSI, Aerodynamic performances, Structural performances

Paper type Research paper

1. Introduction

In turbomachinery, a real blade is often fabricated with a fillet, which is a smooth transition between the blade and the end-wall surfaces. Airflow through the blade root region in an axial compressor is a flow phenomenon influencing aerodynamic performances such as total pressure ratio, adiabatic efficiency and stall margin. Many previous studies confirmed that this geometric feature could reduce endwall loss (or secondary flow loss). Kügeler *et al.* (2008) gave a review of rotor blade fillets' effect in a 15-stage gas turbine compressor. Because of the presence of fillet geometry, there were a flow deflection reduction on the secondary flow and a corner stall decrease at the rotor hub and stator tip. In the comparison with the clean case, the result for the fillet case was a higher throttling range. Matteo (2012) presented the blade fillet effect of an axial 4.5 stage compressor on aerodynamic and structural performances. Since the cross-flow section was declined by fillet geometric feature, the flow deceleration was increased, and the static pressure rose also if the total pressure was reduced. The stress distribution near the

The authors are also grateful to the cooperation between Viettel Aerospace Institute (Vietnam), Hanoi University of Science and Technology, and Le Quy Don Technical University for the support during this research.

Funding: This study was funded by the Foundation for Science and Technology of Le Quy Don Technical University under the grant number 20.1.048.

2049-6427
DOI 10.1108/IJIUS-07-2021-0069

endwall zone was also influenced by the blade fillet. Meyer *et al.* (2012) showed the experimental study on the high-speed compressor cascade without fillets and on three others with different fillet radii (1, 3 and 5 mm). On the suction side, the fillets generated higher losses in the middle of the passage than in the side-wall region. On the pressure side, additional losses in the corner area were produced by adding drag of theses fillets. The effects of impeller blade fillets on aerodynamic performance were detected numerically in Oh (2016). At the corner of the hub pressure surface, there was a small scraping vortex in the case of clean blades, but this vortex disappeared in the case with blade fillets. The Oh's study also demonstrated that the compressor performances dropped in the cause of shroud passage vortex, which grew toward the impeller exit with a higher vortex core in the case with blade fillets than in the case without fillets. Kanjirakkad (2017) showed the experimental study of fillet radius' effects on the secondary flow modification and the generation of the losses under a low Reynolds number. It has been indicated that the presence of a uniform blade fillet decreased the overturning secondary flow and declined marginally the endwall and mass averaged losses.

In fluid–structure interaction (FSI) problems, there are reciprocal influences between one (or more) solid structures and the surrounding (or internal) fluid flow. Numerous researchers applied the FSI approach to analysis study parameters in the turbomachine field such as pressure distribution, equivalent stress, rotor deflection, etc. Lerche *et al.* (2012) predicted stresses on the blades of a single-stage centrifugal compressor by using the one-way FSI method. There was a good agreement between numerical and experimental results when trying to determine a cause of failure. Wang *et al.* (2014) presented a one-way FSI simulation on a 2-MW offshore wind turbine blades to define the mechanical properties for the full machine, such as stress and strain. These values gained a nice result in comparing with other scholar's figures, such as Chen *et al.* (2013). An evaluation matching total pressure ratio, efficiency, and stress between optimum and initial design of a NASA Rotor 37 was introduced by Song *et al.* (2015). The results using one-way FSI method showed that while total pressure ratio was constant, the adiabatic efficiency increased by 0.3% and the maximum stress decreased to 0.9 MPa. However, the authors did not talk about the influence of rotor rotation speed on the stress calculations. Applying FSI analysis and response surface method, Kang and Kim (2016) submitted an optimum impeller design of a centrifugal compressor. At constant pressure, there were an efficiency increment by 1% and a stress decrement by 10% in the case of optimum design compared to the initial design. Dinh *et al.* (2020a) investigated the effects of rotor airflow bleed on aerodynamic and structural performances of a single-stage transonic axial compressor, NASA Stage 37, by using the FSI analysis. The numerical results were validated with the experiment data and showed the small growth of aerodynamic performances, such as about 0.09 and 0.51% increment in peak adiabatic efficiency and total pressure ratio, respectively, at peak efficiency condition. In the case of a reference bleeding airflow, there was a very small rise in von Mises stress and a decrease in total deformation on rotor tip leading edge in span-wise direction as compared to the results of smooth casing.

In the studies indicated above, Matteo (2012) did not valid the numerical fluid results of two models, i.e. the original compressor model and the fillet model, with experimental data. Moreover, the structural model in Matteo (2012), which using the unstructured mesh was automatically generated by the program, was only carried out in the case with fillet. Meanwhile, Dinh *et al.* (2020a) did not survey the influence of fillet radius on the compressor performances. Therefore, the present paper deal with the one-way FSI method to determine the effects of blade fillet in the aerodynamic and structural performances of a single-stage transonic axial compressor, NASA Stage 37. First, to prove the aerodynamic analysis, the fluid model of this compressor is solved by using three-dimensional Reynolds Averaged Navier–Stokes (3D RANS) equations with the k-ε turbulence model. Second, to conduct the structural analysis, the blade surfaces of NASA Stage 37 structural model, such as blade tips, pressure sides and suction sides, carry the pressure load from the fluid model. Finally, the aerodynamic performance results (i.e. total pressure ratio, adiabatic efficiency, stall margin) are validated with experiment data. Due to the lack of experimental figures, the structural performance results (i.e. equivalent von Mises stress, total deformation) are compared between the models without fillet radius and the ones with fillet.

2. Numerical analysis

2.1 Compressor model

Reid and Moore (1978) took an experimental research of the single-stage transonic axial compressor, NASA Stage 37, which had 36 rotor blades rotating at a speed of 17,185.7 rpm for 100% speed design and 46 stator blades. The tip clearance values of this compressor were 0.4 mm under the rotor shroud and 0.762 mm over the stator hub. At peak adiabatic efficiency condition, where adiabatic efficiency was 84.00%, the total pressure ratio and mass flow rate had values of 2.00 and 20.74 kg/s, respectively. The figures of adiabatic efficiency and mass flow rate declined in the order to 79.30% and 19.6 kg/s, while the total pressure ratio reached a peak at 2.093 at near-stall condition. The reference data for temperature and pressure were correspondingly 288.15 K and 101.325 Pa. After the tests of Reid and Moore (1978) on NASA Stage 37, Dunham (1998) investigated an isolated rotor blade, NASA Rotor 37, with an additional geometry of 2.5 mm for a blade hub fillet radius. To facilitate comparisons of results between the clean blade case and the blade fillet case, the stator shroud radius is chosen as rotor hub radius (i.e. 2.5 mm). Figure 1 shows the 3D view of NASA Stage 37 model, where the main design geometries were described in Reid and Moore (1978).

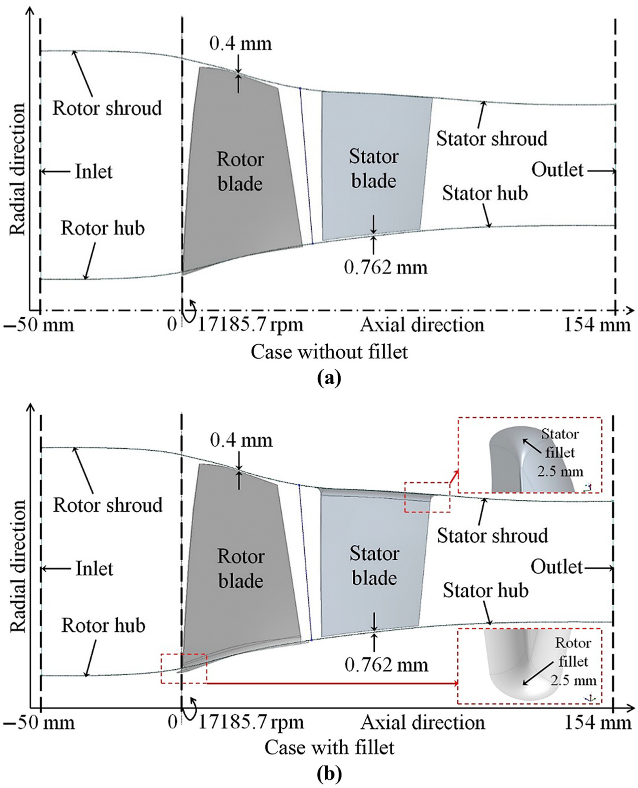

Figure 1.
Meridional view of NASA Stage 37

2.2 Numerical fluid simulation

In the aerodynamic analysis, the 3D RANS equations with the k-ε turbulence model equations were solved using ANSYS CFX 19.1 (ANSYS, 2018a). The computational flow mesh of NASA Stage 37, as shown in Figure 2, was automatically created by using ANSYS TurboGrid, where the rounded symmetric star topologies were applied for the leading edge and trailing edge zones. ANSYS CFX-Pre, CFX-Solver and CFX-Post were individually used to setup the boundary conditions, to solve the main equations and to show the post-process results.

Air ideal gas was chosen as a material of the working fluid. An average static pressure was set for steady state simulation at the stator outlet boundary. A turbulence intensity of 5% was specified at the rotor inlet boundary. The adiabatic smooth wall condition is an option for the surfaces of blades, shrouds and hubs. The general grid interface (GGI) method was used to connect the mesh between the stator and rotor domains. The frozen rotor method using specified pitch angles (360°/36 = 10° for rotor and 360°/46 = 7.826° for stator) was applied at the interface between the rotor outlet and stator inlet surfaces. The two-equation turbulence model k-ε with a scalable wall function was used with $y+$ value of the first nodes near the walls in a range from 20 to 100.

In the next section, an optimal numerical fluid grid for the original compressor model was selected from four cases before validating simulation results with experiment data. In this paper, the computational flow nodes for the clean case and the fillet case were total 851,193 nodes (including 483,183 nodes for rotor, 368,010 nodes for stator) and total 865,232 nodes (including 493,128 nodes for rotor, 372,104 nodes for stator), respectively.

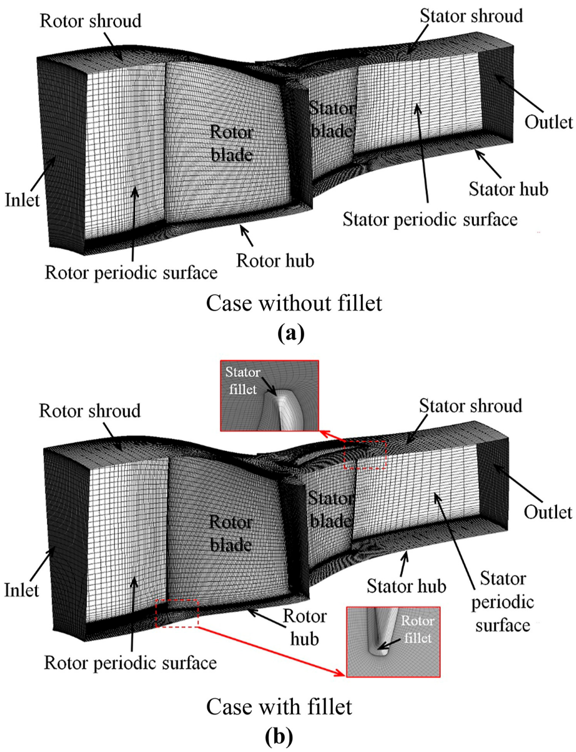

Figure 2.
Computational flow mesh of NASA Stage 37

The aerodynamic performance parameters in this study are the total pressure ratio (PR), adiabatic efficiency (η), stall margin (SM), which are described by Kim *et al.* (2011, 2013a, b), Dinh *et al.* (2015, 2017a), and Dinh and Kim (2017), as shown in the following equations:

$$\mathrm{PR} = \frac{p_{t,out}}{p_{t,in}} \tag{1}$$

$$\eta = \frac{\left(\frac{p_{t,out}}{p_{t,in}}\right)^{\frac{\gamma-1}{\gamma}} - 1}{\frac{T_{t,out}}{T_{t,in}} - 1} \times 100\% \tag{2}$$

$$\mathrm{SM} = \left(\frac{\mathrm{PR}_{\mathrm{stall}}}{\mathrm{PR}_{\mathrm{peak}}} \times \frac{\dot{m}_{\mathrm{peak}}}{\dot{m}_{\mathrm{stall}}} - 1\right) \times 100\% \tag{3}$$

2.3 Numerical structural simulation

In the structural analysis, the blade structures, which were imported from Design-Modeler, were affected by the pressure loads from the aerodynamic simulation results. The titanium alloy (Weiler, 1981; Ermatchenko and Kashaev, 2011) with the density of 4,620 kg/m^3, tensile and compressive yield strength of 930 MPa, and tensile ultimate strength of 1,070 MPa were used for rotor blades. The structural steel (Linden, 2001; Aziaka *et al.*, 2014) with the density of 7,850 kg/m^3, tensile and compressive yield strength of 250 MPa and tensile ultimate strength of 460 MPa were used for stator blades. The structural models, as shown in Figure 3, of this compressor were solved using ANSYS Mechanical 19.1 (ANSYS, 2018b). The rotor blade had a rotational velocity at 100% speed design, i.e. 17,185.7 rpm, but the rotor hub surface and the stator shroud surface were fixed support. The computational structural nodes for the clean case and the fillet case in this research were total 44,156 nodes (including 28,669 nodes for rotor, 15,487 nodes for stator) and total 45,124 nodes (including 28,669 nodes for rotor, 16,455 nodes for stator), correspondingly.

The structural performance parameters in this research are the total deformation (U) and von Mises stress (σ_e), which are described in Mechanical User's Guide (ANSYS, 2018b), as shown in the following equations:

$$U = \sqrt{U_x^2 + U_y^2 + U_z^2} \tag{4}$$

$$\sigma_e = \left[\frac{(\sigma_1 - \sigma_2)^2 + (\sigma_2 - \sigma_3)^2 + (\sigma_3 - \sigma_1)^2}{2}\right]^{1/2} \tag{5}$$

where the principal stresses are always ordered such that $\sigma_1 > \sigma_2 > \sigma_3$.

3. Results and discussion

3.1 Grid-dependency test

Table 1 shows four different grid systems, which was carried out with the aim of finding the optimal case for the compressor model without fillet. The last converged point, where the total pressure ratio reaches the maximal value, was determined as the near-stall condition using the convergence criteria by Chen and Jaw (1998). The performance curves were constructed by increasing the average static pressure at the stator outlet boundary from the

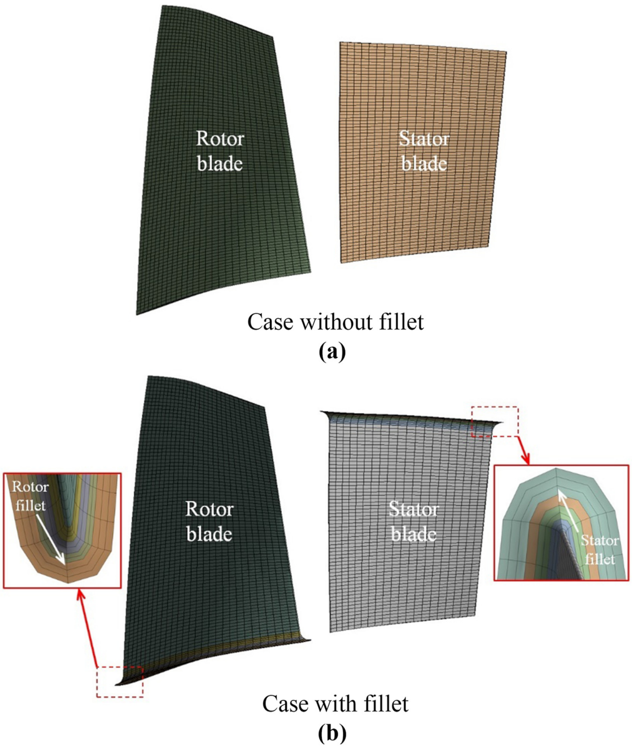

Figure 3.
Computational structure mesh of NASA Stage 37

Table 1.
Different grid systems

Case	Case 1	Case 2	Case 3	Case 4
Rotor nodes	292,550	370,415	483,183	656,602
Stator nodes	218,708	281,116	368,010	497,568
Stage nodes	511,258	651,531	851,193	1,154,170

choking condition (0 Pa) to the last stable convergence point. The simulation was carried out on PC utilizing 55/56 cores of [Dual CPU] Intel Xeon E5-2680 v4 @ 2.40 GHz, where most operating points took approximately 2 h to finish but this increased to over 3.5 h at near-stall condition.

Figure 4 exemplifies the NASA Stage 37 model convergence history of all variables, which turned down rapidly in about the first 200 accumulated time step values and then fluctuated around the RMS's value of 10^{-5}, corresponding the Chen and Jaw's (1998) convergence criteria.

The monitor points display the variation values of pressure ratio and adiabatic efficiency at all time step and at the 100 most recent time step values as shown in Figure 5. According to Chen and Jaw's (1998) documentation, pressure ratio and adiabatic efficiency need vary less than 0.3% per 100 steps. In fact, the pressure ratio variation got a modification of 0.01519%, while the adiabatic efficiency had a change of 0.06815% at peak adiabatic efficiency condition

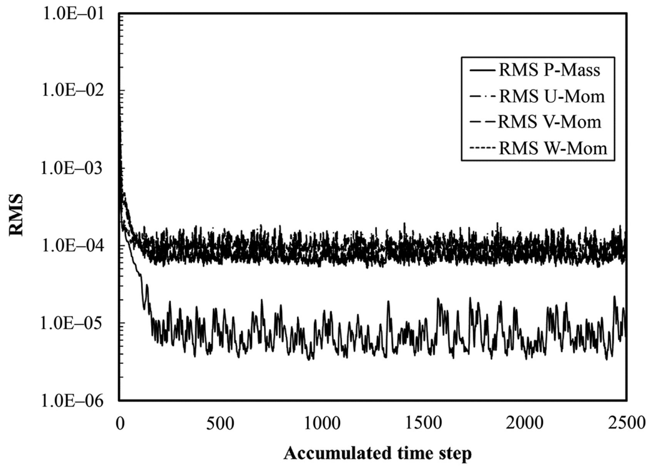

Figure 4.
Root mean square residuals of mass and momentum at peak adiabatic efficiency condition in the original design

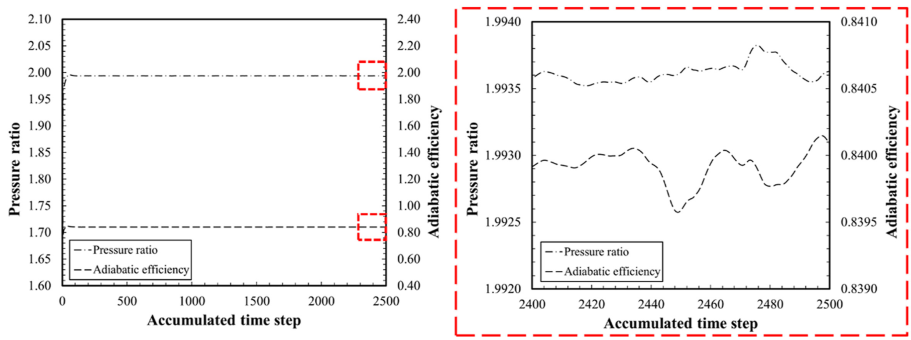

Figure 5.
Monitor points of pressure ratio and adiabatic efficiency at peak adiabatic efficiency condition in the original design

in the case without fillet. Consequently, these two values have satisfied the convergence criteria.

Figure 6 illustrates the numerical results of these different grid systems in compressor map. While the stage nodes increased from case 1 to case 4, normalized mass flows tended to decline from 0.95769 in mesh 1 to 0.93244 in mesh 4. Compared to normalized mass flow at near-stall condition in Reid and Moore (1978) (as shown in Table 2, it was 0.93645), the case 3 and case 4 got a rate of 0.94029 and 0.93244, i.e. the differences were 0.41 and 0.43%, respectively. Thus, mesh 3 was selected as the optimum grid system (total 85,1193 nodes, including 483,183 nodes for rotor, 368,010 nodes for stator) in this study.

3.2 Validation of numerical results

The experimental data of the NASA Stage 37, reported by Reid and Moore (1978), were also used to validate the numerical simulation in the clean blade case. Figure 7a presents the performance curves of total pressure ratio and adiabatic efficiency obtained from numerical simulation in the comparison with several experimental points. This figure show that the numerical simulation was able to closely produce the data from the experiment.

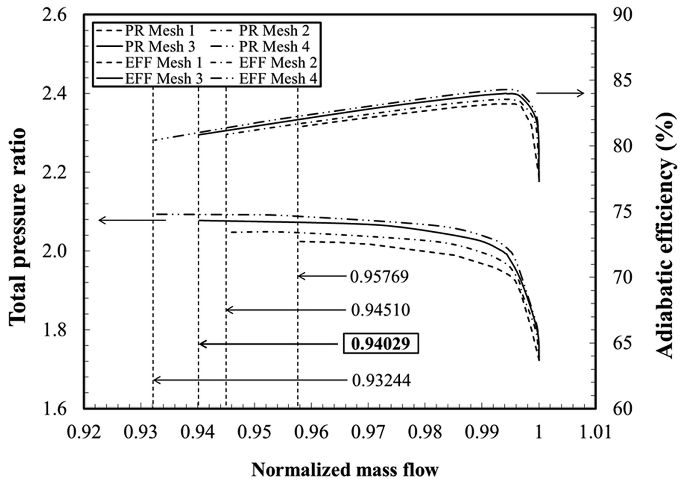

Figure 6.
Compressor map of different grid systems

Table 2.
Overall performance for Stage 37 in Reid and Moore (1978)

Design point	Normalized mass flow	Pressure ratio	Efficiency (%)	Condition
1	1	1.753	81.4	Choking mass flow
2	0.99522	1.879	83.4	
3	0.99092	2.000	84.0	Near peak efficiency
4	0.97611	2.078	82.1	
5	0.93645	2.093	79.3	Near stall

The simulated peak adiabatic efficiency is 84.01%, which is only slightly larger than the measurement, at 84.00%. In addition, the predicted total pressure ratio at peak efficiency condition is 1.99363, which is very close to the experimental result of 2.000. The compressor reached near-stall condition at 94.029% of the main choking mass flow rate, which is very close to the measured result, 93.645%. The predicted stall margin and experimental stall margin are also very similar, 10.21% compared to 10.00%. After the validation, the computational mesh of the clean blade case could apply for the case with fillet radius.

3.3 Case with blade fillet

After validation of the case without fillet with the experimental data, the simulation results in the case of blade fillet 2.5 mm, as shown in Figure 7b, were comprised with the figure of the clean blade. This image presents a large extension of normalized mass flow as the blade fillet delayed the near-stall condition from 0.94029 (clean case) to 0.90992 (fillet case) with a small decline of adiabatic efficiency from 84.01% (clean case) to 83.93% (fillet case). At peak adiabatic efficiency condition, the original design provided a superior total pressure ratio to that of the reference design (1.97721 compared to 1.99363). The blade fillet design extended the stall margin to 15.10%, which is 47.89% higher than that of the clean case (10.21%). In more detail, Table 3 gives the aerodynamic simulation values of this compressor in comparison with the experiment data.

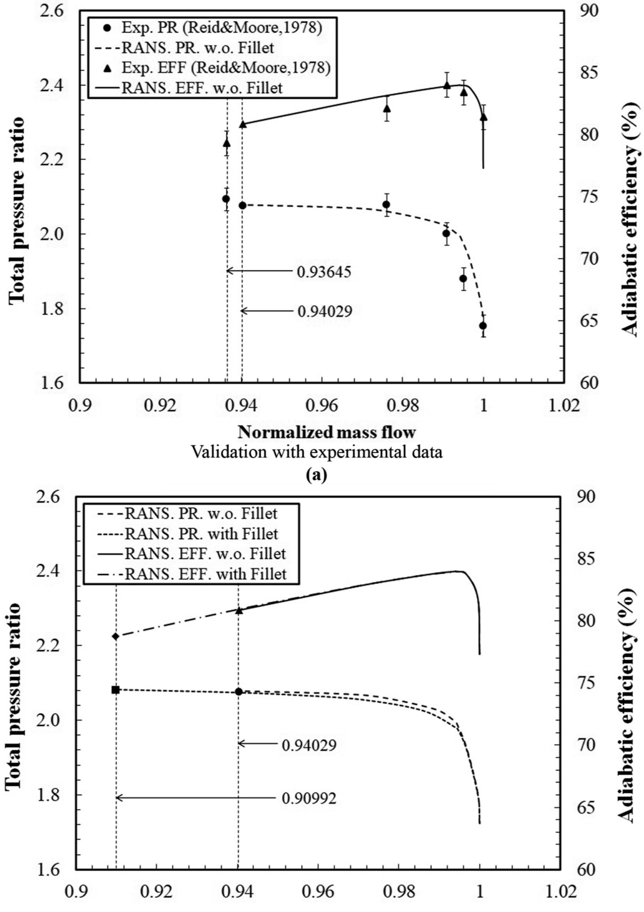

Validation with experimental data
(a)

Comparison between 2 cases
(b)

Figure 7. Compressor maps for validation and comparison purposes

Case	Total pressure ratio Peak efficiency	Near-stall	Normalized mass flow Peak efficiency	Near-stall	Stall margin (%)
Experiment (Reid and Moore, 1978)	2.00000	2.09300	0.99092	0.93645	10.00
Without fillet	1.99363	2.07798	0.99421	0.94029	10.21
With fillet	1.97721	2.08228	0.99449	0.90992	15.10

Table 3. Fluid performance results

At near-stall condition, Figure 8 illustrates the Mach number contours on 98% span surface of NASA Stage 37 with several low-speed zones, corresponded to Mach number of 0.4. The first low-speech zones existing near the rotor leading edge area were significantly reduced

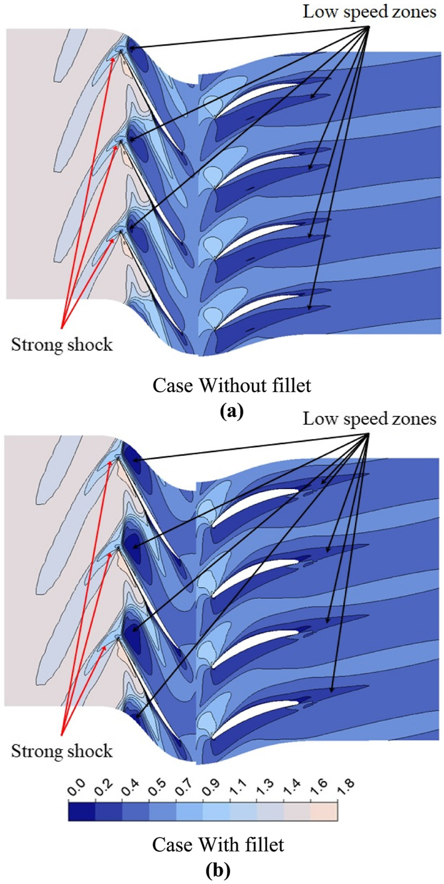

Figure 8.
Relative Mach number contour at 98% span at near-stall condition

from the clean case (Figure 8a) to the fillet case (Figure 8b). The second low-speech zones located around two sides of stator had two independent little zones in the case without fillet (Figure 8a) and were combined into one bigger zone in the remaining case (Figure 8b). This merger could be explained by the effect of fillet radius in the second case, where the airflow was continuous.

Moreover, there was also a strong shock attached at the leading-edge of rotor blade as shown in Figure 8. This shock, as description in Dunham (1998), was interacted strongly with the suction side boundary layer of rotor blade. Therefore, this boundary layer after the shock might separate up to the trailing edge or reattach before this edge. This interesting phenomenon, which was simulated in Dinh *et al.* (2017b, 2020a, b), Vuong *et al.* (2019, 2021) and Pham *et al.* (2020a, b), is demonstrated in Figure 9, where the surface streamlines are separated or reattached on the rotor blade suction side at peak adiabatic efficiency condition. In both cases, the separation line seemed to split the rotor blade suction surface into two parts, as shown in Figure 9. In the left region, the airflow direction was parallel to the axis, but it rolled up or was direction parallel to the separation line in the right region. The fillet case had a smaller scroll line area and more reattachment points in comparison with the clean case.

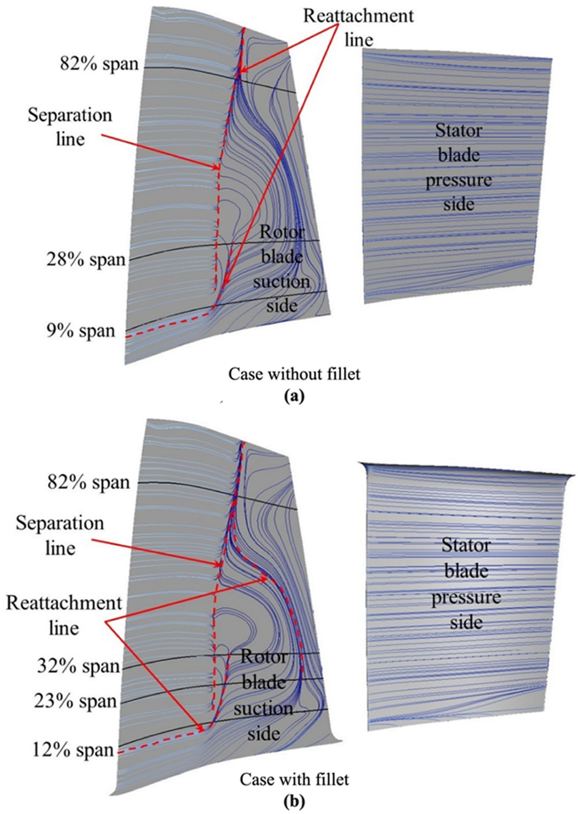

Figure 9.
Blade streamlines at peak adiabatic efficiency condition

Figure 10 shows how the airflow change from the leading-edge zone to the trailing-edge zone on the rotor blade pressure side. In fact, on the rotor hub surface, i.e. 0% span, due to the clean case had a sharp leading-edge, the streamlines were concentrated with a denser density than the ones in the fillet case. In opposition to the leading-edge zone, in the rotor blade trailing-edge zone, the airflow tending to get closer to the rotor blade pressure side appeared densely because of the fillet effect.

In the clean case, a transition from blade surface to the end-wall surface is sudden, but the fillet can make this transition smoother in the reference design. This explains why airflow had a steadier state in the rotor blade trailing-edge zone in the case with fillet, as shown on Figure 11. Figures 8–11 provide the reasons for the enhancement of stall margin of a single-stage transonic axial compressor when the blade fillet is added.

Figures 12 and 13 and Table 4 give some structural performance results. At peak efficiency condition, the maximal equivalent von Mises stress for the clean case, as shown in Figure 12, were considerably greater than for the fillet case, 326.44 MPa for rotor, 72.37 MPa for stator and 271.22 MPa for rotor, 58.92 MPa for stator, respectively. In both cases, the maximal equivalent von Mises stress located on the leading-edge of the transition zone between blades and rotor hub or stator shroud. This shows the rationality in the relationship between the computational fluid dynamics (CFD) and the computational structural mechanics (CSM) simulations. For example, in the rotor blade

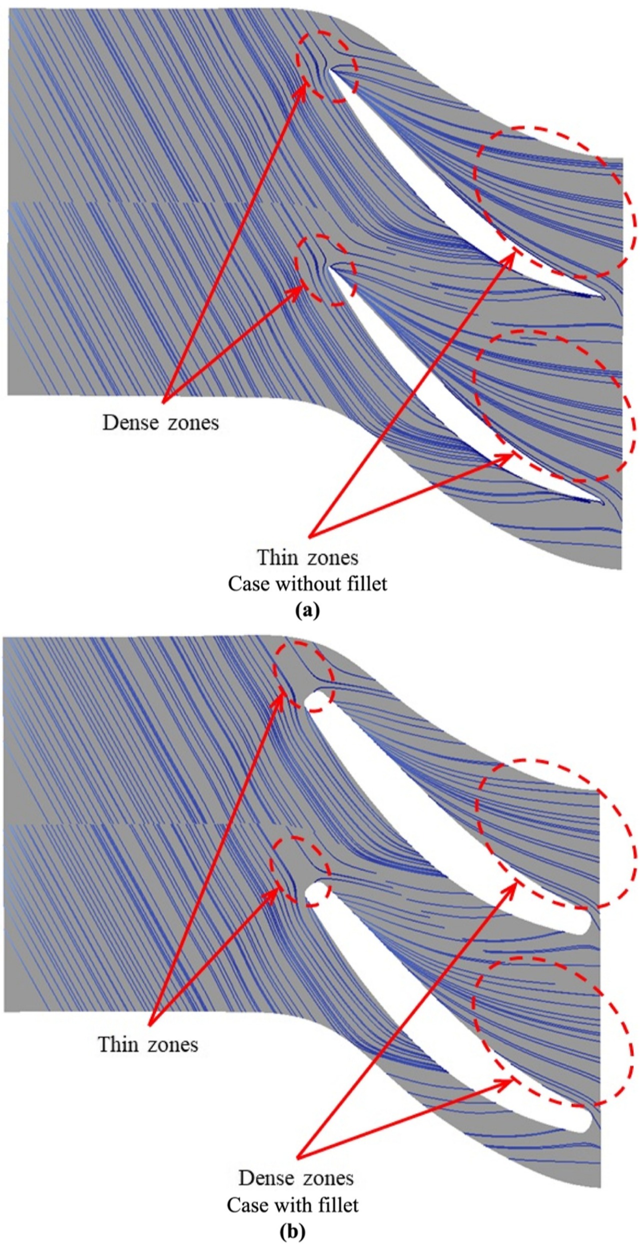

Figure 10.
Rotor hub streamlines at peak adiabatic efficiency condition

trailing-edge zone, where the airflow concentrated with a denser density in CFD simulation, this location in CSM simulation also had the maximal stress. Moreover, the slight change of the maximum stress position from rotor hub surface (in the clean case) to the rotor fillet surface (in the study case) confirmations that the fillets reduce the peak

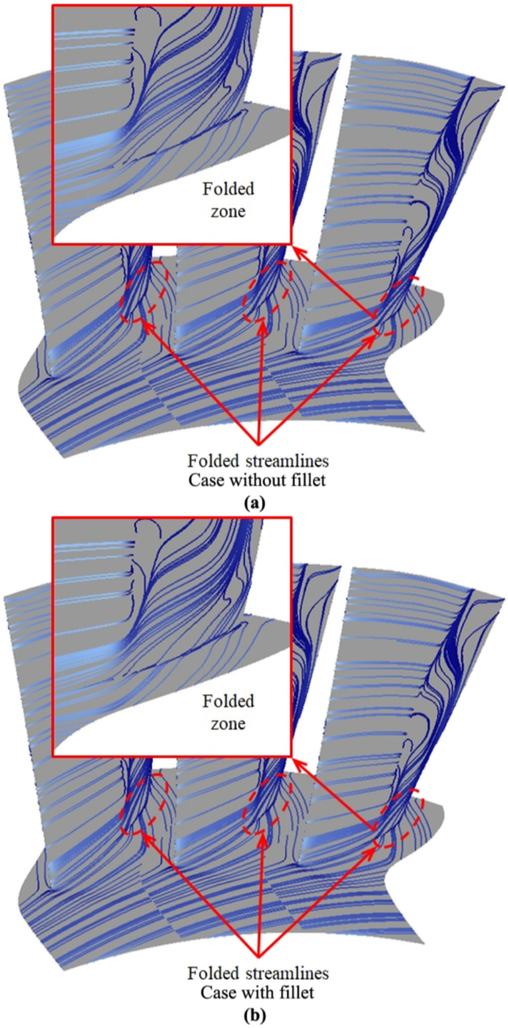

Figure 11.
Streamlines on rotor blade and hub at peak adiabatic efficiency condition

stress value in the blade. It means thus that the additional geometry, i.e. the blade fillet, can help to avoid the extension of the crick inside the blade itself. This is in perfect agreement with the image of the blade crick in the fillet surface, which is illustrated on page 95 of the Matteo's master thesis (Matteo, 2012).

Figure 13 displays the total deformation at peak efficiency condition, where the maximal total deformations in the case with fillet were smaller than in the case without fillet, were in turn 1.2438 mm for rotor, 0.0897 mm for stator and 1.2849 mm for rotor, 0.0995 mm for stator. In both cases, the maximal values are placed on the tip of leading-edge for rotor and stator.

Table 4 provides the values of the maximal equivalent von Mises stress and the maximal total deformation also at near-stall condition. In fact, all structural results at near-stall condition were slightly larger than the structural outcomes at peak adiabatic efficiency condition.

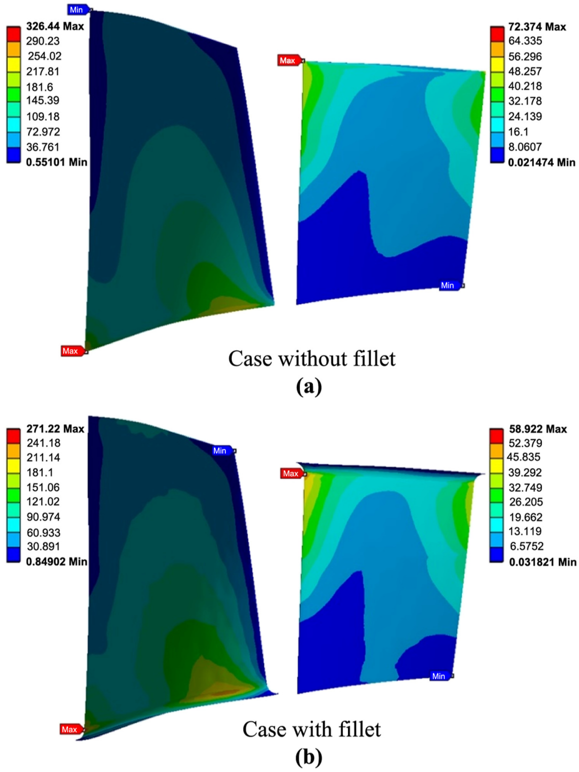

Figure 12.
Equivalent von Mises stress at peak adiabatic efficiency condition

4. Conclusion

The aerodynamic performances of a single-stage transonic axial compressor, NASA stage 37 with an additional geometry, i.e. blade fillet of 2.5 mm, were evaluated by using 3-D RANS analysis. The CFD simulation results indicated that the reference design, i.e. the case with fillet, significantly delays the near-stall point from normalized mass flow rate of 0.94029 in the clean case to normalized mass flow rate of 0.90992. The results for total pressure ratio and adiabatic efficiency at peak efficiency condition in the fillet case were declined by 0.823 and 0.095%, respectively. The stall margin in the clean case is increased by 47.89% in the fillet case. Therefore, with regard to aerodynamic outcomes, total pressure ratio and adiabatic efficiency are almost unchanged while stall margin is enlarged with an additional geometry.

The maximal equivalent von Mises stress of original design were considerably higher than the ones of reference case, by 16.92% for rotor and by 18.59% for stator at peak efficiency condition. The maximal total deformation of the case without fillet were also greater than the ones of the case with fillet, by 3.20% for rotor and by 9.91% for stator at peak efficiency condition. Consequently, regarding the structural performances, maximal equivalent von Mises stress and total deformation are reduced in the fillet case. In addition, the design with blade fillet also helps to avoid broadening the crick inside the blade because the greatest stress position has now moved to the fillet surface.

Based on the obtained results, there are some potential points for the future work, such as to optimize the geometry value of fillet radius, to analysis the two-way FSI, to find the better mesh for fluid model and structural model, to combine blade fillet with blade tip clearance

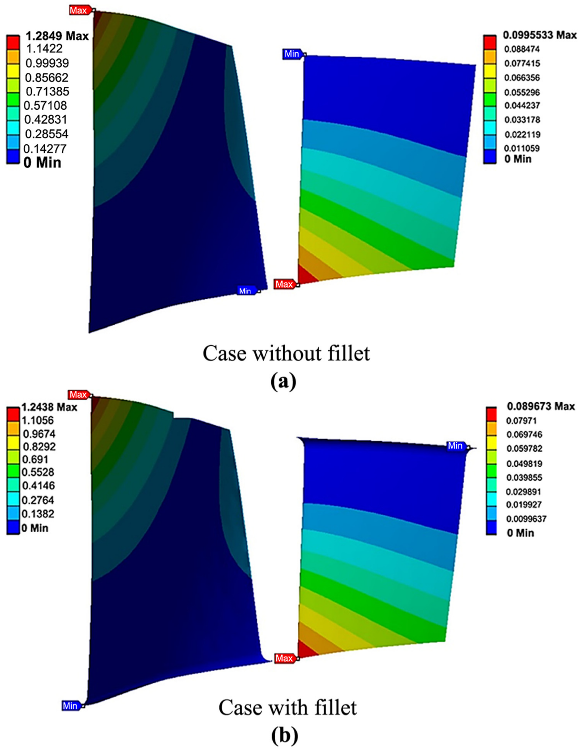

Figure 13. Total deformation at peak adiabatic efficiency condition

Case		Maximal von-Mises stress (MPa) Peak efficiency	Near-stall	Maximal total deformation (mm) Peak efficiency	Near-stall
Without fillet	Rotor	326.44	328.77	1.2849	1.4054
	Stator	72.37	81.53	0.0995	0.1176
With fillet	Rotor	271.22	273.73	1.2438	1.3659
	Stator	58.92	72.55	0.0897	0.1105

Table 4. Structural performance results

treatment, etc. In addition, this approach can be applied to centrifugal compressors, to multi-stage axial compressors or to axial turbines.

Nomenclature

CFD	Computational fluid dynamics
CSM	Computational structural mechanics
EFF	Adiabatic efficiency (%)
FSI	Fluid–structure interaction
GGI	General grid interface
PR	Pressure ratio
RANS	Reynolds averaged Navier–Stokes
RMS	Root mean square

SM	Stall margin (%)
in	Inlet
max	Chocking mass flow point
peak	Peak adiabatic efficiency point
out	Outlet
stall	Near-stall point
γ	Specific heat ratio
η	Adiabatic efficiency (%)
σ_e	von Mises stress
$\dot{m}_{max}$	Mass flow rate at chocking condition
$\dot{m}_{peak}$	Mass flow rate at peak efficiency condition
$\dot{m}_{stall}$	Mass flow rate at near-stall condition
P_t	Total pressure
PR_{peak}	Total pressure ratio at peak efficiency condition
PR_{stall}	Total pressure ratio at near-stall condition
R_F	Blade fillet radius
T_t	Total temperature
U	Total deformation

References

ANSYS (2018a), *ANSYS CFX-Solver Theory Guide*, ANSYS 19.1, ANSYS.

ANSYS (2018b), *Mechanical User's Guide*, ANSYS 19.1, ANSYS.

Aziaka, D.S., Osigwe, E.O. and Lebele-Alawa, T. (2014), "Structural and conceptual design analysis of an axial compressor for a 100 MW industrial gas turbine (IND100)", *World Journal of Mechanics*, Vol. 4, pp. 332-347, doi: 10.4236/WJM.2014.411033.

Chen, C.J. and Jaw, S.Y. (1998), *Fundamentals of Turbulence Modeling*, Taylor & Francis, Washington, DC.

Chen, J., Wang, Q., Shen, W.Z., Pang, X., Li, S. and Guo, X. (2013), "Structural optimization study of composite wind turbine blade", *Materials and Design*, Vol. 46, pp. 247-255, doi: 10.1016/j.matdes.2012.10.036.

Dinh, C.T. and Kim, K.Y. (2017), "Effects of non-axisymmetric casing grooves combined with airflow injection on stability enhancement of an axial compressor", *International Journal of Turbo and Jet-Engines*, Vol. 36 No. 3, pp. 283-296, doi: 10.1515/tjj-2016-0077.

Dinh, C.T., Heo, M.W. and Kim, K.Y. (2015), "Aerodynamic performance of transonic axial compressor with a casing groove combined with blade tip injection and ejection", *Aerospace Science and Technology*, Vol. 46, pp. 176-187, doi: 10.1016/j.ast.2015.07.006.

Dinh, C.T., Ma, S.M. and Kim, K.Y. (2017a), "Effects of stator shroud injection on the aerodynamic performance of a single-stage transonic axial compressor", *Transactions of the Korean Society of Mechanical Engineers B*, Vol. 41 No. 1, pp. 9-19, doi: 10.3795/KSME-B.2017.41.1.009.

Dinh, C.T., Ma, S.B. and Kim, K.Y. (2017b), "Effects of a circumferential feed-back channel on aerodynamic performance of a single-stage transonic axial compressor", in *Proceedings of the ASME Turbo Expo 2017: Turbomachinery Technical Conference and Exposition*, Turbomachinery. Charlotte, North Carolina, Vol. 2A, doi: 10.1115/gt2017-63536.

Dinh, C.T., Vu, D.Q. and Kim, K.Y. (2020a), "Effects of rotor bleeding airflow on aerodynamic and structural performances of a single stage transonic axial compressor", *International Journal of Aeronautical and Space Sciences*, Vol. 21, pp. 599-611, doi: 10.1007/s42405-019-00239-5.

Dinh, C.T., Vuong, T.D., Le, X.T., Nguyen, T.M. and Nguyen, Q.H. (2020b), "Aeromechanic performance of a single-stage transonic axial compressor with recirculation-bleeding channels", *Australian Journal of Mechanical Engineering*. doi: 10.1080/14484846.2020.1832727.

Dunham, J. (1998), "CFD validation for propulsion system components, AGARD-AR-355", p. 11, p. 227, available at: https://www.sto.nato.int/publications/AGARD/AGARD-AR-355/AGARD-AR-355.pdf.

Ermatchenko, A.G. and Kashaev, R.M. (2011), "Production of aircraft engine compressor rotor discs with desired service life in titanium alloys", *Materials Physics and Mechanics*, Vol. 11, pp. 118-125, available at: https://www.ipme.ru/e-journals/MPM/no_21111/kashaev.pdf.

Kang, H.S. and Kim, Y.J. (2016), "Optimal design of impeller for centrifugal compressor under the influence of one-way fluid–structure interaction", *Journal of Mechanical Science and Technology*, Vol. 30 No. 9, pp. 3953-3959, doi: 10.1007/s12206-016-0807-0.

Kanjirakkad, V. (2017), "Experimental study of endwall flow in a low-speed linear compressor cascade: effect of fillet radius", *International Journal of Turbines and Sustainable Energy*, Vol. 1 No. 1, pp. 1-7, doi: 10.4273/ijtse.1.1.01.

Kim, J.H., Choi, K.J. and Kim, K.Y. (2011), "Optimization of a transonic axial compressor considering interaction of blade and casing treatment to improve operating stability", doi: 10.1115/GT2011-45404.

Kim, J.H., Choi, K.J. and Kim, K.Y. (2013a), "Aerodynamic analysis and optimization of a transonic axial compressor with casing grooves to improve operating stability", *Aerospace Science and Technology*, Vol. 29 No. 1, pp. 81-91, doi: 10.1016/j.ast.2013.01.010.

Kim, J.H., Kim, D.W. and Kim, K.Y. (2013b), "Aerodynamic optimization of a transonic axial compressor with a casing groove combined with tip injection", *Proceedings of the Institution of Mechanical Engineers, Part A: Journal of Power and Energy*, Vol. 227 No. 8, pp. 869-884, doi: 10.1177/0957650913503311.

Kügeler, E., Nürnberger, D., Weber, A. and Engel, K. (2008), "Influence of blade fillets on the performance of a 15 stage gas turbine compressor", *ASME Turbo Expo 2008: Power for Land, Sea, and Air*, Vol. 6 Nos Turbomachinery, Parts A, B, and C, pp. 415-424, doi: 10.1115/gt2008-50748.

Lerche, A.H., Moore, J.J., White, N.M. and Hardin, J. (2012), "Dynamic stress prediction in centrifugal compressor blades using fluid structure interaction", *Oil and Gas Applications; Concentrating Solar Power Plants, Steam Turbines; Wind Energy*. Vol. 6, doi: 10.1115/gt2012-69933.

Linden, D.H. (2001), "Corrosion control in industrial axial flow compressor", in *Proceeding of the 30th Turbomachinery Symposium, Texas A&M University*, Turbomachinery Laboratories, pp. 115-120, available at: https://oaktrust.library.tamu.edu/bitstream/handle/1969.1/163342/t30pg115.pdf.

Matteo, P. (2012), *Structural and Fluid-Dynamic Analysis of an Axial Compressor with Adjustable Inlet Guide Vanes*, Master of Science, Matriculation No. 1034265, Department of Industrial Engineering, Faculty for Engineering, University of Padova, Italy.

Meyer, R., Schulz, S., Liesner, K., Passrucker, H. and Wunderer, R. (2012), "A parameter study on the influence of fillets on the compressor cascade performance", *Journal of Theoretical and Applied Mechanics*, Vol. 50, pp. 131-145, available at: http://www.ptmts.org.pl/jtam/index.php/jtam/article/download/v50n1p131/104.

Oh, J.J. (2016), "The effects of blade fillets on aerodynamic performance of a high-pressure ratio centrifugal compressor", in *International Compressor Engineering Conference, Paper 2396*, available at: https://docs.lib.purdue.edu/icec/2396/.

Pham, K.Q., Nguyen, Q.H., Vuong, T.D. and Dinh, C.T. (2020a), "Parametric study on aerodynamic performance of a single-stage transonic axial compressor with recirculation-bleeding channels", *International Journal of Fluid Machinery and Systems*, Vol. 13 No. 2, doi: 10.5293/IJFMS.2020.13.2.348.

Pham, K.Q., Le, X.T. and Dinh, C.T. (2020b), "Effects of stator splitter blades on aerodynamic performance of a single-stage transonic axial compressor", *Journal of Mechanical Engineering and Sciences*, Vol. 14 No. 4, pp. 7369-7378, doi: 10.15282/jmes.14.4.2020.05.0579.

Reid, L. and Moore, R.D. (1978), "Performance of single-stage axial-flow transonic compressor with rotor and stator aspect ratios of 1.63 and 1.78, respectively, and with design pressure ratio of 1.82", NASA TP-1659, available at: https://ntrs.nasa.gov/citations/19790001889.

Song, Y.J., Kang, H.S. and Kim, Y.J. (2015), "Reliability evaluation of an axial compressor rotor using fluid-structural interaction analysis", in *3rd International Conference on Materials and Reliability*, Jeju island, South Korea.

Vuong, T.D., Dinh, D.M., Dinh, C.T. and Bui, X.L. (2019), "Aerodynamic performance of a single-stage transonic axial compressor using recirculation-bleeding channels", *Journal of Science and Technology*, Vol. 138, pp. 033-037, available at: https://jst.hust.edu.vn/journals/jst.138.khcn.2019.29.7.7.

Vuong, T.D., Kim, K.Y. and Dinh, C.T. (2021), "Recirculation-Groove coupled casing treatment for A transonic axial compressor", *Aerospace Science and Technology*, Vol. 111, 106556, ISSN: 1270-9638, doi: 10.1016/j.ast.2021.106556.

Wang, Z.K., Tsai, G.C. and Chen, Y.B. (2014), "One way fluid–structure interaction simulation of an offshore wind turbine", *International Journal of Engineering and Technology Innovation*, Vol. 4 No. 3, pp. 127-137, available at: https://ojs.imeti.org/index.php/IJETI/article/view/137.

Weiler, W. (1981), "Compressor rotor wheel and Method of making same", U.S. Patent, 4273512, available at: https://patentimages.storage.googleapis.com/0e/1d/76/dba12d9f8520ed/US4273512.pdf.

Corresponding author
Hoang-Quan Chu can be contacted at: chu.h-quan.fas@lqdtu.edu.vn